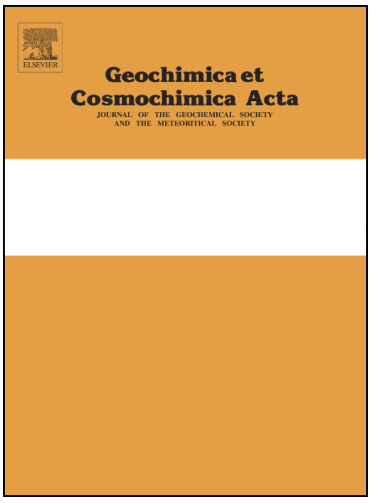

Noble gas elemental abundances in three solar wind regimes as recorded by the Genesis mission

Nadia Vogel, Veronika S. Heber, Peter Bochsler, Donald S. Burnett, Colin Maden, Rainer Wieler

PII: S0016-7037(19)30505-8
DOI: https://doi.org/10.1016/j.gca.2019.08.007
Reference: GCA 11386

To appear in: *Geochimica et Cosmochimica Acta*

Received Date: 22 January 2019
Accepted Date: 7 August 2019

Please cite this article as: Vogel, N., Heber, V.S., Bochsler, P., Burnett, D.S., Maden, C., Wieler, R., Noble gas elemental abundances in three solar wind regimes as recorded by the Genesis mission, *Geochimica et Cosmochimica Acta* (2019), doi: https://doi.org/10.1016/j.gca.2019.08.007

Noble gas elemental abundances in three solar wind regimes as recorded by the Genesis mission

Nadia Vogel[a,*], Veronika S. Heber[a,b,**], Peter Bochsler[c], Donald S. Burnett[d], Colin Maden[a], Rainer Wieler[a,***]

[a] ETH Zürich, Institute for Geochemistry and Petrology, Department of Earth Sciences, Clausiusstrasse 25, CH-8092 Zürich, Switzerland

[b] Department of Earth and Space Sciences, University of California, Los Angeles, CA 90095-1567, USA

[c] Physikalisches Institut, University of Bern, Sidlerstrasse 5, CH-3012 Bern, Switzerland

[d] California Institute of Technology, Division of Geological and Planetary Sciences, Pasadena, CA 91125, USA

* current address: Amt für Abfall, Wasser, Energie und Luft, Stampfenbachstrasse 12, CH-8090, Zürich, Switzerland

** current address: Paul Scherrer Institute, Division for Radiation Safety and Security, 5232 Villigen PSI, Switzerland

*** corresponding author: wieler@erdw.ethz.ch

accepted for publication in Geochimica & Cosmochimica Acta

August 12, 2019

Abstract

We discuss elemental abundances of noble gases in targets exposed to the solar wind (SW) onboard the "Genesis" mission during the three different SW "regimes": "Slow" (interstream, IS) wind, "Fast" (coronal hole, CH) wind and solar wind related to coronal mass ejections (CME). To this end we first present new Ar, Kr, and Xe elemental abundance data in Si targets sampling the different regimes. We also discuss He, Ne, and Ar elemental and isotopic abundances obtained on Genesis regime targets partly published previously. Average Kr/Ar ratios for all three regimes are identical to each other within their uncertainties of about 1% with one exception: the Fast SW has a 12% lower Xe/Ar ratio than do the other two regimes. In contrast, the He/Ar and Ne/Ar ratios in the CME targets are higher by more than 20% and 10%, respectively, than the corresponding Fast and Slow SW values, which among themselves vary by no more than 2-4%.

Earlier observations on lunar samples and Genesis targets sampling bulk SW wind had shown that Xe, with a first ionisation potential (FIP) of ~12 eV, is enriched by about a factor of two in the bulk solar wind over Ar and Kr compared to photospheric abundances, similar to many "low FIP" elements with a FIP less than ~10 eV. This behaviour of the "high FIP" element Xe was not easily explained, also because it has a Coulomb drag factor suggesting a relatively inefficient feeding into the SW acceleration region and hence a depletion relative to other high FIP elements such as Kr and Ar. The about 12% lower enrichment of Xe in Genesis' Fast SW regime observed here is, however, in line with the hypothesis that the depletion of Xe in the SW due to the Coulomb drag effect is overcompensated as a result of the relatively short ionisation time of Xe in the ion-neutral separation region in the solar chromosphere. We will also discuss the rather surprising fact that He and Ne in CME targets are quite substantially enriched (by 20% and 10%, respectively) relative to the other solar wind regimes, but that this enrichment is not accompanied by an isotopic fractionation. The Ne isotopic data in CMEs are consistent with a previous hypothesis that isotopic fractionation in the solar wind is mass-dependent.

Introduction

The solar wind represents a sample from the Sun's outer convective zone, which in turn is the best proxy for the composition of the primordial solar nebula. The goal of NASA's Genesis mission thus was to measure the isotopic composition and elemental abundances of a wide range of elements trapped from the solar wind in a variety of targets exposed in space for ~2.3 years (Burnett and team, 2011; Burnett, 2013). For noble gases and a few other elements, isotopic and to a limited extent elemental compositions of the solar wind are also obtained with lunar and some asteroidal regolith samples as well as the aluminum foils exposed during the Apollo lunar landings (e. g., Eberhardt et al., 1970; Pepin et al., 1970; Hintenberger et al, 1974; Geiss et al., 1972, 2004; Fueri et al., 2015; Wieler, 2016). High precision noble gas and nitrogen data on Genesis samples were reported by Heber et al. (2009, 2012), Marty et al., (2010, 2011),

Vogel et al. (2011a), Pepin et al. (2012), Crowther and Gilmour (2013), and Meshik et al. (2014); see Wieler (2016) for a summary.

For the derivation of solar atmospheric abundances from solar wind abundance data, isotopic as well as elemental fractionation effects which arise upon injection and acceleration of solar wind ions need to be understood. This was a major reason for the Genesis mission to sample ions not only from the "bulk solar wind" but also from different solar wind "regimes" (Neugebauer et al., 2003; Burnett and team, 2011). These are High-speed (here called "Fast", speeds typically in the 500-800 km/s range) solar wind from coronal holes, Low-speed ("Slow", typically 250 – 500 km/s) solar wind from interstream flows and solar wind from Coronal Mass Ejections ("CME"). Isotopic fractionation effects are well constrained for noble gases and nitrogen (e. g. Heber et. al. 2009, 2012; McKeegan et al., 2011; Marty et al., 2011). Of particular importance for the present work are the data presented by Heber et al. (2012) on elemental and isotopic abundances of He, Ne, and Ar in Fast and Slow SW targets. Relative to the lighter isotopes of each element, the heavier isotopes are depleted in the Slow SW relative to the Fast SW, and the depletion factor decreases strongly with increasing atomic mass from 63.1 ‰/amu for He, 4.2 ‰/amu for Ne to 2.6 ‰/amu for Ar. These numbers are in good agreement with values predicted by a model which explains the fractionation as the result of inefficient Coulomb drag upon solar wind acceleration (Bodmer and Bochsler, 1998, 2000). This model is briefly explained in the Appendix and further addressed in the Discussion section. For Kr and Xe, the inefficient Coulomb drag model predicts very small isotopic fractionation effects, well below the precision to be expected for our analyses of the small amounts of these heavy noble gases in Genesis targets.

In this paper, we focus mainly on the elemental fractionation of noble gases between Sun and solar wind. We do this first by analysing the elemental abundances of the three heavy noble gases in the three regimes sampled by Genesis. In particular, we present data for ^{36}Ar, ^{84}Kr, and ^{132}Xe in 6 to 7 individual Genesis silicon (Si) targets from each of the three regimes. Furthermore we also address the elemental abundances of He, Ne, and Ar measured by Heber et al. (2012) in the other set of Genesis regime targets mentioned in the previous paragraph, reporting here in addition the full data set on CME targets not comprehensively published in that paper. This data set allows us to identify some significant differences - as well as many similarities - in the elemental abundance pattern of the noble gases sampled by the different Genesis regimes. In a broader perspective, including also abundance data of non-noble gas elements from in-situ analyses (Reisenfeld et al., 2013), we then address other observations and theories on elemental fractionations of different elements in the solar wind.

For the rest of this section we discuss various mechanisms proposed to fractionate the solar wind composition relative to the composition at its source. It has long been known that various mechanisms in the source and acceleration regions affect the *elemental* composition of the solar wind differently in different flow regimes. The best-known case is the strongly variable helium abundance (Robbins et al., 1970; Borrini et al., 1981; Bürgi and Geiss, 1986). Underlying physical mechanisms for fractionating the abundances are disputed. While H^+ and He^{++} stream at equal speeds in the low, collision-dominated solar atmosphere, their velocity distributions ultimately de-couple at higher altitudes in the more tenuous corona. Borrini et al. (1981) occasionally found strong depletions of helium in solar wind emanating along current sheets. They tentatively ascribed these helium-poor features to particularly high de-coupling points of H^+ and He^{++} in a strongly stratified corona with large depletions of helium at high altitude.

Bürgi and Geiss (1986) emphasized the role of inefficient drag induced by weak Coulomb coupling as responsible for the general depletion of He in the solar wind. Bürgi (1992) investigated three-fluid models of the solar wind theoretically in more detail and identified Coulomb coupling between He and H as an agent to stabilize the solar wind momentum flux. More recently, Laming et al. (2017) challenged this interpretation, arguing that there is little evidence for inefficient Coulomb drag depleting helium in the solar wind. These latter authors favor explanations based on the particularly high first ionisation potential of He, as discussed next.

It is generally accepted that besides the differential acceleration of pre-existing ions, the ionisation process of elements itself is also a key ingredient in feeding minor species from the solar atmosphere into the solar wind and thus shaping the (elemental) composition of the solar wind: Elements with a first ionisation potential (FIP) below about 10 eV are enriched by factors of between ~1.5 - 4 (Meyer, 1993) relative to elements with higher FIP, depending on the solar wind regime (FIPs of elements relevant in the following can be read off Fig. 5). As an exception, also the high-FIP element Xe is enhanced in the bulk SW by a factor of 2 – 2.5 relative to solar abundances. Such an enhancement was first postulated with lunar regolith samples (Wieler and Baur, 1995) and later confirmed with Genesis targets that sampled the bulk solar wind (Vogel et al., 2011a). The inferred solar abundances of heavy noble gases are explained in the Discussion chapter. Geiss and Bochsler (1985), Marsch et al. (1995) and Geiss (1998) argued that in the chromosphere the actual parameter governing the "FIP effect" is the standard *first ionisation time* of elements (FIT), i. e. the average time it takes to ionise a neutral species under chromospheric conditions (see Geiss and Bochsler, 1985; Marsch et al., 1995 for exact definitions). FIT is closely related to FIP. Xe has a short ionisation time compared to those of other elements with a similar FIP (e. g. C, O, N, Kr, Ar) , particularly if electronic collisions in hot, shocked chromospheric gas play a role in the first ionisation of neutrals. Xenon with its large electronic envelope is thus more sensitive to ionisation under such dynamic circumstances than other high-FIP elements, which provides an explanation for its overabundance in the solar wind.

Experimental

Analytical procedures for the Ar, Kr, and Xe analyses in regime targets were essentially identical to those described by Vogel et al. (2011a) for the bulk SW targets, with the main challenge being the fact that noble gas concentrations were a factor of about three lower in the regime targets. This was partly compensated by analysing the gases from an on average roughly 1.5 times larger surface aera. We also restricted the measurements to one major isotope only of each element. In the following we summarize the major analytical topics and refer to Vogel et al. (2011a) and references therein for details.

All samples analysed in this work for ^{36}Ar, ^{84}Kr, and ^{132}Xe (Table 1) are Czochralski-grown Si (CZ-Si; Jurewicz et al., 2003). At NASA's Johnson Space Center Genesis Curation Laboratory, the samples had been cleaned to remove "brown stain", a molecular organic film with a mean thickness of ~40 Å deposited on the target surfaces in space (Allton et al., 2006). The fraction of solar wind Ar, Kr, and Xe trapped within this film and hence lost prior to analysis is negligible (Heber et al., 2009). Surface particle contamination was also removed at the Curation laboratory. Non-flown targets used to determine material blanks were treated analogously.

Prior to noble gas extraction, samples were pre-heated in vacuum for several days at 130 °C to remove adsorbed atmospheric noble gases. Significant losses of Ar, Kr, or Xe during pre-heating can be excluded (Vogel et al., 2011a). Noble gases were then released by UV laser ablation (λ = 213 nm) with up to 20 pulses/s and pulse durations of 3-5 ns. Extracted sample surface areas are shown in Table 1; other laser extraction parameters are identical to those given by Vogel et al. (2011a). Each area was extracted twice, leading to total extraction times of about 30 - 60 minutes. Quantitative gas release was checked by re-extractions of already ablated sample areas. During extraction, gases were continuously cleaned by admission to a stainless steel finger attached to the sample chamber and held at -80 °C. Gases were then further purified by admission to several Ti-Zr getters.

Ar, Kr, and Xe were frozen onto charcoal at the temperature of boiling N_2, allowing us to pump off He and Ne. The three heavy gases were then analysed together as described by Vogel et al. (2011a). Restricting the analyses to one isotope only of each gas (^{36}Ar, ^{84}Kr, ^{132}Xe) also helped to reduce uncertainties related to the extrapolation of ion current signals to gas inlet time.

The low sample gas amounts required frequent "procedural blank" and "material blank" analyses, i. e. simulating a sample gas extraction procedure without firing the laser and analysing the gases released by the laser from non-flown but otherwise identical (including pre-heating) CZ-Si pieces, respectively. All sample and material blank extractions were first corrected for procedural blanks. In a second step, sample signals were corrected for the procedural blank-corrected material blanks, which were additionally scaled to the extracted area of each sample. Procedural blanks were in the following ranges (atoms of ^{36}Ar, ^{84}Kr, ^{132}Xe, respectively): (2.4±0.6) * 10^6, 10200±6100, 8200±4200. Since no systematic dependence of these values with "extraction" times used for the blank analyses was observed (30 - 60 minutes, as for samples), we correct all samples with the averages of all procedural blanks. Procedural blanks were the dominant blank source for Ar and Xe, i. e. the corrected material blank values did not exceed ~30% of the average procedural Xe blank signal and were zero within uncertainties for Ar. For Kr, corrected material blank values were in a similar range as the procedural blanks. Resulting total blank corrections for the various samples are in the following ranges (in % of the sample gas amounts for ^{36}Ar, ^{84}Kr, and ^{132}Xe, respectively): <0.1, 0.7 - 1.8, 4-12. We assign an uncertainty of 50% to the blank corrections based on the scatter of the blank values within each analysis run. Mass spectrometer sensitivities were determined with pure calibration gases as described by Heber et al. (2009) and Vogel et al. (2011a).
Uncertainties of the data for individual samples as given in Table 1 include ion statistics, blank corrections and mass spectrometer sensitivity variations. For gas concentrations, an additional 2% uncertainty for the size of the extracted area was quadratically added. Because we are mainly interested in differences in elemental fractionations between different regimes, we do not include the uncertainties of the standard gas amounts (2%, 5%, 5% for Ar, Kr, and Xe concentrations and 5% for elemental ratios, respectively; Heber et al., 2009). Note that the extrapolation of individual Xe ion current readings to gas inlet time was slightly ambiguous for a few analyses due to remaining traces of chemically active gases introduced into the spectrometer together with the sample gases. As is discussed in more detail by Vogel et al. (2011a), during the first few readings active gases sometimes released relevant amounts of "memory Xe" from previous samples or calibration analyses, until these active gases had completely been removed by the getters in the mass spectrometer flight tube. Together with the blank correction, the somewhat uncertain Xe memory correction is the major source of uncertainty of the Xe concentrations and the ^{132}Xe/^{36}Ar ratios. This will also be discussed in the Results section.

The He, Ne, and Ar data from diamond on silicon (DOS) targets discussed in this paper had mostly been reported earlier by Heber et al. (2012). DOS is an amorphous Diamond-like carbon film deposited On a Silicon substrate. Analytical procedures were similar to those applied in this work and by Vogel et al. (2011a), with further details given by Heber et al. (2012). DOS is an ideal target to collect light noble gases, as it has a very low diffusivity even for He and hence quantitatively retains all noble gases (Heber et al., 2009). The low atomic mass of carbon also minimizes backscatter losses of the implanted light noble gases.

Results

Ar, Kr, and Xe data for individual Si targets as well as average values are given in Table 1 (preliminary averages based on a subset of these data were presented by Vogel et al., 2011b). Data are reported as fluxes of the respective isotope derived from the concentrations (number of atoms per ablated unit area) measured in each target and exposure durations given in the footnote of the table. No backscatter loss correction was required, as the maximum backscatter loss of ^{36}Ar from Si is predicted to be 0.1% for a very low solar wind speed of 250 km/s, and will be lower for Kr and Xe and for higher speeds (Heber et al., 2009). Weighted average concentrations and elemental ratios (expressed as ratios of the respective major isotope analysed) given in Table 1 for each regime are calculated with the online tool IsoplotR (Vermeesch, 2018) with stated uncertainties being one σ. The table also lists the bulk solar wind fluxes calculated from the regime averages weighted with the respective exposure durations (CME = 22%, Fast = 38%, Slow = 40%). For comparison, average values from Genesis Si bulk solar wind targets are also shown (Vogel, 2011a). Figs. 1 & 2 display the data given in Table 1.

For all three heavy noble gases, fluxes determined from each individual analysis agree within their two sigma uncertainties with the weighted average flux of the respective regime (Fig. 1; the ^{36}Ar analyses of Fast SW target Nr. 3 was rejected as outlier). Exceptions are the ^{84}Kr data of the Fast SW targets where the Mean Square Weighted Deviation (MSWD, see Table 1) of 2.9 suggests an overdispersion of the data. We therefore adopt as uncertainty of the ^{84}Kr flux of the Fast SW target the standard error of the mean as calculated from the scatter of the individual analyses. The rather low MSWD values of all ^{36}Ar and ^{132}Xe fluxes suggests that our uncertainty estimates for the fluxes of these two isotopes is conservative. The bulk SW flux of ^{132}Xe calculated from the regime data averages agrees very well with the published value (Table 1, Fig. 1c) measured in bulk solar wind CZ-Si targets (Vogel et al., 2011a), while the respective values for ^{36}Ar and ^{84}Kr differ both by about 8%, somewhat more than we would have expected. Fluxes of all three isotopes measured in aluminum bulk SW targets by Meshik et al. (2014) are lower than the values published by Vogel et al. (2011a) by another 8 - 12%.

Table 1 and Figure 2 show the elemental ratios ^{84}Kr/^{36}Ar and ^{132}Xe/^{36}Ar of the individual regime targets as well as the weighted average values. As noted in the Experimental section, the stated errors do not include the systematic uncertainties of the absolute ratios of ~5% due to the standard gas uncertainties. The ^{84}Kr/^{36}Ar ratio from the third analysis of the Fast SW target was rejected, due to the uncertain ^{36}Ar concentration value noted above. All other individual ratios agree within their two sigma uncertainties with the weighted average of the respective regime. The rather low MSWD values of the ^{132}Xe/^{36}Ar ratios of all three regimes

mirror the similarly low MSWD values of the ^{132}Xe fluxes, suggesting that the stated uncertainties of the average ^{132}Xe/^{36}Ar ratios are conservative.

Table 2 gives the average fluxes of ^{4}He, ^{20}Ne, and ^{36}Ar and the ^{4}He/^{36}Ar and ^{20}Ne/^{36}Ar ratios for the Fast and Slow SW based on three individual DOS targets for each regime. The data of each individual analysis are given by Heber et al. (2012). For consistency with the Ar-Xe data in Si targets reported here, also the errors given in Table 2 represent the uncertainties of the weighted averages (rather than the respective standard deviations given by Heber et al., 2012). Table 2 also lists the data of all 3 individual CME regime targets not yet reported by Heber et al. 2012. In Table 3 we give the He, Ne, and Ar isotopic data of the CME targets, which had not been published in Heber et al. (2012) and we repeat the respective average values of the Fast and Slow SW targets, both as absolute values and as permill deviations from the bulk SW ratios. He and Ar in the CME target have an isotopic composition identical to bulk SW values, while Ne isotopes are identical to those in the Fast SW ($(^{20}Ne/^{22}Ne)_{CME}$ = 13.71±0.02; about 5 ‰ lower than the bulk SW value of 13.78 of Heber et al. (2009). The Ne isotopic data are also shown in Fig. 3.

Discussion

The noble gas data in Genesis regime targets presented here can be summarized as follows:

1. Solar wind Ar, Kr, and Xe fluxes are somewhat variable between the different regimes (Fig. 1): For all three elements, weighted average fluxes measured during the Slow SW regime are between ~8 - 24% higher than the averages for the Fast SW regime, and the weighted average fluxes during the CME regime were another ~10-15% higher than those of the Slow SW regime. The weighted Ar, Kr, and Xe fluxes of bulk solar wind calculated from the regime target data agree reasonably well with the values measured earlier with Genesis bulk solar wind targets. In the following subsection, the noble gas fluxes in the different regimes will also be set in relation to the respective SW hydrogen fluxes.

2. Whereas no significant difference is observed for the Kr/Ar ratios in the different regimes, Xe/Ar ratios are regime-dependent (Fig. 2b): The average ^{84}Kr/^{36}Ar ratios of Slow and Fast SW are almost identical to each other and also the average CME value agrees well with those of the other two regimes. In contrast, the average ^{132}Xe/^{36}Ar ratio of the Fast SW regime is lower by ~12% (by almost three sigma) than the average of the Slow SW regime. This difference is clearly significant, the more so given the possibly overestimated uncertainty of the regime-averaged Xe fluxes and ^{132}Xe/^{36}Ar ratios (see Results section). This difference cannot be explained by a putative systematic uncertainty of the material blank correction, since the - substantial - Xe blank correction is dominated by the procedural blank (Results section), which is independent of the sample analysed, while the Ar blank is negligible anyway. Finally, the average CME ^{132}Xe/^{36}Ar ratio agrees with the respective Slow SW value. Also, the ^{84}Kr/^{36}Ar ratio of the bulk solar wind as calculated from the fluence-weighted regime data agrees very well with previously published values based on Genesis bulk solar wind targets. Somewhat less good is the agreement for the bulk SW ^{132}Xe/^{36}Ar ratio, which is about 10% lower when calculated from the regime-based data compared with the direct bulk SW targets. The differences between measured SW values and the inferred solar Xe/Ar ratio (Lodders et al., 2009) also shown in Fig. 2b and Table 1 illustrate the known enrichment of Xe relative to

Ar in the solar wind compared to its abundance in the Sun (e. g. Wieler and Baur, 1995; Vogel et al., 2011a, Meshik et al., 2014). The inferred solar Xe/Ar ratio is also very similar to the measured value in Jupiter's atmosphere (Atreya et al., 2003; Fig. 2b), giving further support for the conclusion that Xe is enriched in the solar wind. The Kr/Ar ratios in all SW regimes also agree well with the inferred solar value and within uncertainty marginally also with the Jupiter value (Fig. 2a), although the latter comparison may also indicate a moderate enrichment of Kr over Ar in the solar wind.

3. Like the Xe/Ar ratios, the He/Ar and Ne/Ar ratios are regime-dependent, as shown in Fig. 4. However, in contrast to Xe/Ar a clear difference of at least 20% and 10%, respectively, is observed between the CME regime on the one hand and Fast and Slow SW on the other, whereas the relative abundances of He, Ne, and Ar in the latter two regimes differ by no more than 2-4 %. Yet, He/Ar and Ne/Ar ratios appear roughly linearly correlated in all three regimes. In contrast to the quite substantial difference in the He, Ne, and Ar abundances between CME and normal solar wind, the isotopic ratios of these three gases in CMEs are remarkably similar to those of the other two regimes (Table 3 & Fig. 3). This latter observation will be discussed next, before we address the elemental abundances of all noble gases in the different regimes.

He, Ne, and Ar isotopes

Heber et al. (2012) noted that the heavy isotope depletion observed for He, Ne, and Ar in the slow SW compared to the fast solar wind is well reproduced by the inefficient Coulomb drag model and that the three Ne isotopes were suggestive for a mass-dependent isotopic fractionation process, as is expected by this model. They therefore applied it to infer the isotopic composition of He, Ne, and Ar in the solar photosphere from their data. The Ne data of Heber et al. (2012) are shown in Fig. 3, together with the final data for CMEs given here. Although uncertainties are large especially for $^{21}Ne/^{22}Ne$, the CME data fall on a fractionation line very similar to the one reported by Heber et al. (2012).

Regime-dependence of solar wind noble gas fluxes

The fluxes and elemental compositions of noble gases in the different solar wind regimes as sampled by Genesis will not be perfectly representative for the "pure" respective regimes (Neugebauer et al., 2003). In particular, the Genesis sampling algorithm was biased to prevent contamination of normal solar wind (fast or slow) from CME-related flows. The composition of the CME target should therefore not be considered to be representative for pure CME-related solar wind, as this target also sampled some normal solar wind. For a comprehensive discussion of the contribution of CMEs to the solar wind see Hundhausen (1997). Table 4 is an attempt to qualitatively evaluate the efficiency of the Genesis regime separation. The upper part of the table displays the noble gas fluxes in the three regimes normalized to the bulk SW values. Also given are proton fluxes determined with the Genesis Ion monitor (GIM, Reisenfeld et al., 2013). The lower part of the table lists the noble gas to proton flux ratios, again normalized to the ratios for bulk SW.

It has been known from in-situ investigations made by space missions that the proton momentum flux (mass flux multiplied with speed) in the (non-CME-related) solar wind is approximately constant over a wide velocity range (e.g., Steinitz and Eyni, 1980; Schwenn, 1983). Hence, the proton flux is lower in fast SW than in slow SW. This is also reflected in the GIM data for the Genesis regimes. Actually, the difference of ~25% between fast and slow proton fluxes seen by the GIM (Table 4) is very similar to the difference measured by Ulysses

for “mean fast” and “mean slow” SW proton fluxes (von Steiger et al., 2010). This suggests that at least with respect to proton fluxes the definition for fast and slow SW regimes used by Genesis and Ulysses agree quite well with each other. Furthermore, Reisenfeld et al. (2013) noted that the Genesis Fast SW sample was enriched in low-FIP elements by a factor of about 1.5 relative to photospheric abundances, an enrichment not much larger than the factor of 1.37 measured by Ulysses for polar coronal holes, which also indicates that the Genesis regime distinction between Fast and Slow SW worked quite well. On the other hand, the He enrichment of ~22% in the Genesis CME target is less pronounced than expected for typical CME-related flows. Neukomm (1998) performed a careful analysis of the composition of 42 CMEs with Ulysses/SWICS. She found an average enhancement in 15 near-equatorial CMEs of He/H compared to fast and slow wind of approximately 38%. Table 4 also shows that absolute noble gas fluxes are slightly lower in the Fast SW than in the Slow SW, but that, relative to protons, the noble gas abundances are somewhat higher in the Fast SW than the Slow SW. Apart from the higher He flux, the CME target also recorded higher fluxes of all other noble gases. Yet, relative to proton fluxes, apart from He only Ne shows a substantial excess of ~14% relative to the bulk SW.

Elemental abundances of noble gases (and other elements) in the solar wind and their regime dependence

We emphasize again that Xe is generally enhanced in all types of solar wind relative to Ar and Kr by typically a factor of 2 - 2.5, if compared to photospheric (source) abundances. Since heavy noble gases cannot be detected with optical methods in the solar atmosphere, and since meteoritic abundances of volatiles can not be used for inferences on the solar composition (Ott, 2014), one has to determine the solar abundances of Ar, Kr, and Xe by interpolation from neighboring non-volatile elements relying on constraints from nucleosynthetic models (see, e.g., Lodders et al. 2009). These interpolations seem fairly reliable and Lodders et al. (2009) estimate the uncertainties of the solar abundance of heavy noble gases to be of the order of 0.1 dex or ~25% (dex(x) = 10^x). As noted above, the inferred solar Xe/Ar ratio is also very similar to the Jovian value (Fig. 2b).

Unlike the He, Ne, and Ar isotopic composition in different solar wind regimes, a Coulomb drag model, which emphasizes differential acceleration, cannot account for the enhanced abundance of Xe in the solar wind. Considering the unfavourable Coulomb drag factor of Xe, it predicts a depletion rather than an enrichment of this element relative to Ar and Kr. The Laming model (Laming et al., 2017), which emphasizes the importance of ionisation processes, predicts a Xe enrichment, but one smaller than observed, unless one appeals to a particularly efficient ionisation of this element in the ion-neutral separation region. We noted in the introduction that the ionisation process of elements is a further key ingredient in feeding minor species from the solar atmosphere into the solar wind and thus shaping the (elemental) composition of the solar wind, with the first ionisation potential (FIP) of elements being a crucial parameter. The most plausible explanation for the Xe enrichment in our view is that its unfavourable Coulomb drag factor is balanced and overcome by its particularly efficient ionisation in the ion-neutral separation region. In simple one-dimensional, stationary models of the solar atmosphere the ion-neutral separation is assumed to be located near the boundary between chromosphere and the transition region, where temperatures reach typically 10^4 K, too low to ionise high-FIP elements by electronic collisions. However, the atmosphere becomes transparent to the coronal extreme ultraviolet (EUV) radiation so that also high-FIP elements

can be ionised. For example, the model of Marsch et al. (1995) predicts an enrichment of Xe over Ar of a factor of two, whereas Kr should be enriched over Ar by a factor of 1.5. The estimates of Marsch et al. (1995) do not strongly depend on conditions in the chromosphere but merely on atomic parameters. We note that the estimates of Marsch et al. (1995) do not consider ionisation of elements by electronic collisions; they are probably best applicable for situations of weak chromospheric activity. However, particularly in the case of Xe electron collisions could be important, especially in regions of shocked, hot and compressed chromospheric gas, i.e., those regions which preferentially feed slow solar wind. This is because Xe has a large electron shell and a comparatively large cross section for electronic collisions. In this context, it seems no surprise that Xe is generally overabundant in the solar wind.

Zahnle et al. (2019) recently discussed a mechanism to efficiently ionise xenon by resonant charge exchange with protons, a mechanism which leaves Xe ions in an excited state, and which to our knowledge has not been considered in FIP/FIT models heretofore. These authors propose this process to facilitate a preferential loss of xenon from the early terrestrial atmosphere (Avice et al., 2018). Zahnle et al. (2019) point out that this process does not work for Kr or the other noble gases. Hence, it seems plausible that xenon could be preferentially ionised compared to other heavy noble gases by resonant charge exchange, leading to a strong enrichment in the solar wind.

The $^{84}Kr/^{36}Ar$ ratio in Genesis Bulk solar wind (Vogel et al., 2011a) and regime targets (this work) of $\sim 4.2 \times 10^{-4}$ is close to the tabulated solar value of 4.05×10^{-4} (Lodders et al., 2009), but an actual enrichment of a factor of 1.5 of Kr over Ar cannot be excluded given the stated uncertainties of solar Ar and Kr abundances of ~20% each and should be considered in view of the arguments made above. Furthermore, as noted above, the Jovian Kr/Ar ratio only marginally agrees with the SW value, allowing for a weak enrichment of Kr over Ar in the solar wind.

In any case, the enrichment of Xe over Ar in the solar wind by a factor of 2 - 2.5 is well established and in agreement with expectations from FIT-separation models. Concerning different regimes, it is generally accepted that the FIT/FIP-effects are stronger in slow wind than in fast wind (cf. Bochsler, 2007). This is indeed supported by one of the two main findings of this study, as we observe a stronger enrichment (by some 12%) of Xe over Ar (and Kr) in slow solar wind. The Genesis regime data thus support the hypothesis that the FIT effect plays a dominant rôle in shaping abundances of heavy noble gases in the solar wind.

In Figure 5, we compare the relative abundances of noble gases measured in three different Genesis regime targets relative to the bulk solar wind composition, including abundances of several low-FIP elements extracted from ACE/SWICS and ACE/SWEPAM data for the exposure periods of the three relevant targets (Reisenfeld et al. 2013). Since fluxes are the largest during periods of slow wind, this regime substantially controls the average bulk solar wind composition and therefore will exhibit the weakest deviations from bulk SW. The depletion of high-FIP elements is less pronounced in high-speed wind, hence, low-FIP elements appear more strongly depleted in the Fast SW target. The patterns of noble gases in all three panels of Fig. 5 follow the general systematics of the in-situ observed elements as reported by Reisenfeld et al. (2013), but unlike the low-FIP elements, they exhibit a smooth dependence on FIP. In particular, our data show that the Ne/Ar ratio in CME-related wind is

higher than in the bulk wind, confirming other studies showing a systematic enhancement in CMEs with increasing FIP.

Less easily understood is the pattern for some other elements in CMEs shown in Fig. 5c: The trend of simultaneous enrichment of low-FIP elements and high-FIP elements compared to medium-FIP elements published by Reisenfeld et al. (2013) and reported earlier by Neukomm (1998) for CMEs emanating from low solar latitudes is clearly confirmed by our new abundances of noble gases in CME-targets (red symbols). It is puzzling that elements with very similar ionisation properties and in a similar mass range such as Mg and Si appear to be fractionated against each other by a factor of the order of 1.3 in the CME-period data from ACE reported by Reisenfeld et al. (2013). The separation of these two low-FIP elements is less pronounced but still obvious in the period of exposures of Slow SW and Fast SW-targets. Heidrich-Meisner et al. (2018) find no significant disparity among Si and Mg abundances in a recent re-evaluation of ACE data. On the other hand, Fe, with a similar FIP as Si and Mg, seems somewhat depleted relative to Mg and Si and relative to photospheric abundances in the data set of Reisenfeld et al. (2013) (their Table 7) as well as in the results for low-speed wind (or periods of high O^{7+}/O^{6+}-ratios) of Heidrich-Meisner et al. (2018). This is an indication that apart from the FIP-related separation also mass-dependence plays a rôle in feeding the solar wind from photospheric matter.

Also not easily understood are the He isotopic data in the CME target. A conventional view for the relatively high He abundance in CMEs is that species with unfavourable Coulomb-drag factors are gradually enriched in regions near closed field lines in the low corona, while those with favourable drag factors are steadily carried away with the solar wind. Occasionally, when a coronal mass ejection occurs, the enriched layers are blown off and can be detected. Doubly charged $^4He^{++}$ has a very unfavourable Coulomb-drag factor, unlike $^3He^{++}$ (Appendix 1). One would therefore expect that, concomitant with the observed ^{4}He-enrichment of approximately 20%, the $^4He/^3$He-ratio would be similarly enhanced by about 20% in CME ejecta, but the isotopic composition of helium in the CME target is normal.

Another possible explanation for the absence of substantial He isotopic variations in CMEs is that He is locally enriched by gravitational settling in low chromospheric strata as an element (i. e. ^{3}He and ^{4}He) and not only as the isotope ^{4}He, due to inefficient ionisation. The enrichment of He in CMEs then could occur when such layers are blown up into the transition region and lower corona, where they are quickly ionised and incorporated into the solar wind flow. The systematics of enhanced abundances of high-FIP elements in CMEs noted above seem to support this hypothesis, but the *simultaneous* enrichments of high- *and* low-FIP elements in coronal mass ejecta, relative to elements with an intermediate first ionisation potential such as oxygen (Fig. 5c), suggests that that this is not the full explanation.

In the case of the Ne isotopes, Heber et al. (2012) found a slight depletion of ^{22}Ne of the order of 1% in low-speed solar wind compared to high-speed wind, which they attributed to inefficient Coulomb drag in typical slow wind. The CME target exhibits no obvious difference in neon isotopic abundances compared to fast wind (Fig. 3). This seems no surprise in view of the dilution effects discussed above and in view of the large diversity of CME compositions observed with in-situ instruments (e. g. Neukomm, 1998; Zurbuchen et al., 2016).

Conclusions

The elemental composition of noble gases in targets exposed by the Genesis mission to solar wind representing three different regimes ("Fast", "Slow", "CME") shows some variability. While Ar/Kr is identical in all regimes, Xe is enhanced relative to Ar (and Kr) in the Slow regime relative to the Fast regime by some 12%. This difference has to be viewed in light of the well-known enrichment of Xe in the bulk solar wind of a factor of 2 - 2.5 relative to elements with a high First Ionisation Potential (including Ar). The two lightest noble gases He and Ne show a different behaviour: their abundances relative to Ar vary by only a few percent between the Fast and Slow regimes, but in the CME targets He and Ne are substantially enriched by more than 20% and 10%, respectively.

The regime-dependent Xe abundance supports the hypothesis that the enrichment of Xe in the solar wind is a consequence of its relatively fast ionisation in the chromosphere, i. e. its short First Ionisation Time, whence enhanced availability for acceleration (cf. Geiss and Bochsler, 1985), since FIT/FIP effects are stronger in slow SW. The clear enrichment of He and Ne in the CME targets (in parallel with a much smaller enrichment of these gases in the slow SW relative to the Fast SW targets) is difficult to explain, as possibly expected elemental fractionations in CMEs due to inefficient Coulomb drag or inefficient ionisiation of ^{4}He in the chromosphere should be accompanied by isotopic fractionations in He and Ne in CMEs that are not observed.

The Ne data for CME published here are in line with the observation by Heber et al. (2012) that the Ne isotopic compositions in the different solar wind regimes are consistent with a mass-dependent fractionation process, in agreement with expectations based on the inefficient Coulomb drag hypothesis. Based on their data Heber et al. (2012) had concluded that the Ne isotopic composition in the Sun is about 1.6%/amu heavier than the bulk solar wind value.

Acknowledgments: We appreciate the great support of the Genesis curation team at the Johnson Space Center, Houston with sample selection and cleaning. Heinrich Baur, Henner Busemann and Rosmarie Neukomm are thanked for technical support and discussions, and we acknowledge the very helpful comments by AE Gregory Herzog and three reviewers. This work was supported by the Swiss National Science Foundation.

Appendix 1: The role of Coulomb drag in the acceleration of minor species in low speed solar wind

Following a hypothesis by Geiss et al. (1970) and Bürgi and Geiss (1982), Bodmer and Bochsler (1998) assumed that heavy test particles are accelerated by large proton fluxes, particularly proton streams with large densities which enable strong coupling between proton and test particles by frequent Coulomb collisions. This situation is encountered in low-speed solar wind.

Bodmer and Bochsler (1998) used a one-fluid model of the solar wind to compute the fractionation factor between two different types of test particles. Near the coronal maximum,

where the temperature gradient vanishes, the momentum balance yields a simple expression for the velocity of a minor species x, v_x

$$v_x = v_p \left(1 - \frac{H_x C_p f(r)}{\Phi_p}\right),$$

with v_p denoting the proton speed, C_p a flux normalization constant, f(r) the flux expansion factor and Φ_p the proton flux. The coupling of a species x (mass A_x, charge Z_x) to protons is described by the Coulomb drag factor H_x

$$H_x = \frac{2A_x - Z_x - 1}{Z_x^2} \sqrt{\frac{A_x + 1}{A_x}}$$

Efficient coupling in dense proton streams requires the speed of test particles to be close to the proton speed. The coupling is most efficient for particles with high charges and, correspondingly, with low H_x. Among the species with the least efficient coupling is $^4He^{++}$, with $H_{4He} = 1.40$.

More generally, the efficiency of Coulomb drag depends strongly on the dominant charge state in the solar wind acceleration region in the inner corona. Table A1 lists a few examples relevant here.

Table A1: Dominant charge states of elements in the solar wind acceleration region and corresponding H-factors

Element/Isotope	**Charge State**	H_x
^{4}He	2+	1.40
^{3}He	2+	0.87
^{16}O	6+	0.72
^{16}O	7+	0.50
^{20}Ne	8+	0.50
^{22}Ne	8+	0.56
^{24}Mg	10+	0.38
^{28}Si	9+	0.58
^{28}Si	10+	0.46
^{28}Si	11+	0.37
^{28}Si	12+	0.30
^{56}Fe	9+	1.27
^{56}Fe	10+	1.02
^{56}Fe	11+	0.83
^{56}Fe	12+	0.69
^{56}Fe	13+	0.59
^{56}Fe	14+	0.50

References

Allton, J.H., Calaway, M.J., Rodriguez, M.C., Hittle, J.D., Wentworth, S.J., Stansbery, E.K., McNamara, K.M., 2006. Genesis solar wind sample curation: a progress report, 37th Lunar and Planetary Science Conference. Lunar and Planetary Institute, Houston, #1611.

Atreya, S.K., Mahaffy, P.R., Niemann, H.B., Wong, M.H., Owen, T.C., 2003. Composition and origin of the atmosphere of Jupiter - an update, and implications for the extrasolar giant planets. Planet. Space Sci. 51, 105-112.

Avice, G., Marty, B., Burgess, R., Hofmann, A., Philippot, P., Zahnle, K., Zakharov, D., 2018. Evolution of atmospheric xenon and other noble gases inferred from Archean to Paleoproterozoic rocks. Geochim. Cosmochim. Acta 232, 82-100.

Bochsler, P., 2007. Minor ions in the solar wind. Astronomy and Astrophysics Review 14, 1-40.

Bochsler, P., Fludra, A., Giunta, A., 2017. Charge states of krypton and xenon in the solar wind. Sol. Phys. 292, 128.

Bodmer, R., Bochsler, P., 1998. Fractionation of minor ions in the solar wind acceleration process. Phys. Chem. Earth 23, 687-692.

Bodmer, R., Bochsler, P., 2000. Influence of Coulomb collisions on isotopic and elemental fractionation in the solar wind acceleration process. J. Geophys. Res-Space Phys. 105, 47-60.

Borrini, G., Gosling, J.T., Bame, S.J., Feldman, W.C., Wilcox J.M., 1981. Solar wind helium and hydrogen structure near the heliospheric current sheet: A signal of coronal streamers at 1 AU. J. Geophys. Res. 86, 4565-4573.

Bürgi, A., 1992. Proton and alpha particle fluxes in the solar wind: Results of three-fluid model. J. Geophys. Res. 97, 3137-3150.

Bürgi, A., Geiss, J., 1986. Helium and minor ions in the corona and solar wind - dynamics and charge states. Sol. Phys. 103, 347-383.

Burnett, D.S., Genesis Sci, T., Wieler, R., Heber, V.S., Vogel, N., Grimberg, A., 2011. Solar composition from the Genesis Discovery Mission. Proc. Natl. Acad. Sci. U. S. A. 108, 19147-19151.

Burnett, D.S., 2013. The Genesis solar wind sample return mission: Past, present, and future. Meteorit. Planet. Sci. 48, 2351-2370.

Crowther, S.A., Gilmour, J.D., 2013. The Genesis solar xenon composition and its relationship to planetary xenon signatures. Geochim. Cosmochim. Acta 123, 17-34.

Eberhardt, P., Geiss, J., Graf, H., Grögler, N., Krähenbühl, U., Schwaller, H., Schwarzmüller, J., Stettler, A., 1970. Trapped solar wind noble gases, exposure age and K/Ar-age in Apollo 11 lunar fine material. Proc. Apollo 11 Lunar Sci. Conf., 1037-1070.

Füri, E., Barry, P.H., Taylor, L.A., Marty, B., 2015. Indigenous nitrogen in the Moon: constraints from coupled nitrogen-noble gas analyses of mare basalts. Earth Planet. Sci. Lett. 431, 195-205.

Geiss, J., 1998. Constraints on the FIP mechanisms from solar wind abundance data. Space Sci. Rev. 85, 241-252.

Geiss, J., Bochsler, P., 1985. Ion composition in the solar wind in relation to solar abundances. In: Proc. Conf. Isotopic Ratios in the Solar System (Cepadues-Editions, Toulouse, France), 213-228.

Geiss, J., Hirt P., Leutwyler H. (1970). On acceleration and motion of ions in corona and solar wind. Sol. Phys. 12, 458-483.

Geiss, J., Bühler, F., Cerutti, H., Eberhardt, P., Filleux, C., 1972. Solar wind composition experiment. Apollo 16 Prelim. Sci. Rep., NASA SP-315, 14.11-14.10.

Geiss, J., Bühler, F., Cerutti, H., Eberhardt, P., Filleux, C., Meister, J., Signer, P., 2004. The Apollo SWC experiment: results, conclusions, consequences. Space Sci. Rev. 110, 307-335.

Heber, V.S., Wieler, R., Baur, H., Olinger, C., Friedmann, T.A., Burnett, D.S., 2009. Noble gas composition of the solar wind as collected by the Genesis mission. Geochim. Cosmochim. Acta 73, 7414-7432.

Heber, V.S., Baur, H., Bochsler, P., McKeegan, K.D., Neugebauer, M., Reisenfeld, D.B., Wieler, R., Wiens, R.C., 2012. Isotopic mass fractionation of solar wind: evidence from fast and slow solar wind collected by the Genesis mission. Astrophys. J. 759, 121.

Heber, V.S., McKeegan, K.D., Bochsler, P., Burnett, D.S., Guan, Y., Reisenfeld, D.B., Wieler, R., 2013. Elemental fractionation processes in the solar wind revealed by Genesis solar wind regime samples. 44th Lunar and Planetary Science Conference. Lunar and Planetary Institute, Houston, #3028.

Heber, V.S., McKeegan, K.D., Bochsler, P., Duprat, J., Burnett, D.S., 2014. The elemental composition of solar wind with implications for fractionation processes during solar wind formation, 45th Lunar and Planetary Science Conference. Lunar and Planetary Institute, Houston, #2117.

Heidrich-Meisner, V., Berger, L., Wimmer-Schweingruber, R.F., 2018. Disparity among low first ionization potential elements. Astronomy & Astrophysics 619, A79.

Hintenberger, H., Weber, H.W., Schultz, L., 1974. Solar, spallogenic, and radiogenic rare gases in Apollo 17 soils and breccias. Proc. Lunar Sci. Conf. 5th, 2005-2022.

Hundhausen, A. J., 1997. Coronal Mass Ejections. in: Cosmic Winds and the Heliosphere (J. R. Jokipii, C. P. Sonett, and M. S. Giampapa, eds.) University of Arizona Press, 259-296.

Jurewicz, A.J.G., Burnett, D.S., Wiens, R.C., Friedmann, T.A., Hays, C.C., Hohlfelder, R.J., Nishiizumi, K., Stone, J.A., Woolum, D.S., Becker, R., Butterworth, A.L., Campbell, A.J., Ebihara, M., Franchi, I.A., Heber, V., Hohenberg, C.M., Humayun, M., McKeegan, K.D., McNamara, K., Meshik, A., Pepin, R.O., Schlutter, D., Wieler, R., 2003. The Genesis solar-wind collector materials. Space Sci. Rev. 105, 535-560.

Kerridge, J.F., 1980. Secular variations in composition of the solar wind: evidence and causes, in: Pepin, R.O., Eddy, J.A., Merrill, R.B. (Eds.), Proc. Conf. Ancient Sun. Pergamon, New York, pp. 475-489.

Laming, J.M., Heber, V.S., Burnett, D.S., Guan, Y., Hervig, R., Huss, G.R., Jurewicz, A.J.G., Koeman-Shields, E.C., McKeegan, K.D., Nittler, L.R., Reisenfeld, D.B., Rieck, K.D., Wang, J., Wiens, R.C., Woolum, D.S., 2017. Determining the Elemental and Isotopic Composition of the Pre-solar Nebula from Genesis Data Analysis: The Case of Oxygen. Astrophysical Journal Letters 851.

Lodders, K., Palme, H., Gail, H.P., 2009. Abundances of the elements in the solar system. In: Springer Materials - The Landolt-Börnstein Database (ed. J. E. Trümper), Springer Berlin-Heidelberg, 1-59.

Mahaffy, P.R., Niemann, H.B., Alpert, A., Atreya, S.K., Demick, J., Donahue, T.M., Harpold, D.N., Owen, T., 2000. Noble gas abundance and isotope ratios in the atmosphere of Jupiter from the Galileo Probe Mass Spectrometer. J. Geophys. Res. 105, 15061-15071.

Marsch, E., von Steiger, R., Bochsler, P., 1995. Element Fractionation By Diffusion In the Solar Chromosphere. Astronomy & Astrophysics 301, 261-276.

Marty, B., Chaussidon, M., Wiens, R.C., Jurewicz, A.J.G., Burnett, D.S., 2011. A ^{15}N-poor isotopic composition for the solar system as shown by Genesis solar wind samples. Science 332, 1533-1536.

Marty, B., Zimmermann, L., Burnard, P.G., Wieler, R., Heber, V.S., Burnett, D.L., Wiens, R.C., Bochsler, P., 2010. Nitrogen isotopes in the recent solar wind from the analysis of Genesis targets: Evidence for large scale isotope heterogeneity in the early solar system. Geochim. Cosmochim. Acta 74, 340-355.

McKeegan, K.D., Kallio, A.P.A., Heber, V.S., Jarzebinski, G., Mao, P.H., Coath, C.D., Kunihiro, T., Wiens, R.C., Nordholt, J.E., Moses, R.W., Reisenfeld, D.B., Jurewicz, A.J.G., Burnett, D.S., 2011. The oxygen isotopic composition of the Sun inferred from captured solar wind. Science 332, 1528-1532.

Meshik, A.P., Hohenberg, C.M., Pravdivtseva, O.V., Mabry, J.C., Allton, J.H., Burnett, D.S., 2009. Relative Abundances of Heavy Noble Gases from the Polished Aluminum Solar Wind Collector on Genesis, 40th Lunar and Planetary Science Conference. Lunar and Planetary Institute, Houston, #2037.

Meshik, A., Hohenberg, C., Pravdivtseva, O., Burnett, D., 2014. Heavy noble gases in solar wind delivered by Genesis mission. Geochim. Cosmochim. Acta 127, 326-347.

Meyer, J.P., 1993. Element fractionation at work in the solar atmosphere. In: Origin and Evolution of the Elements, (eds. N. Prantzos, E. Vangioni-Flam and M. Casse), Cambridge Univ. Press, 26-62.

Neugebauer, M., Steinberg, J.T., Tokar, R.L., Barraclough, B.L., Dors, E.E., Wiens, R.C., Gingerich, D.E., Luckey, D., Whiteaker, D.B., 2003. Genesis on-board determination of the solar wind flow regime. Space Sci. Rev. 105, 661-679.

Neukomm, R.O., 1998. Composition of Coronal Mass Ejections derived with SWICS/Ulysses. PhD Thesis, Univ. Bern, Switzerland, 135pp.

Ott, U., 2014. Planetary and pre-solar noble gases in meteorites. Chemie der Erde 74, 519-544.

Pepin, R.O., Nyquist, L.E., Phinney, D., Black, D.C., 1970. Isotopic composition of rare gases in lunar samples. Science 167, 550-553.

Pepin, R.O., Schlutter, D.J., Becker, R.H., Reisenfeld, D.B., 2012. Helium, neon, and argon composition of the solar wind as recorded in gold and other Genesis collector materials. Geochim. Cosmochim. Acta 89, 62-80.

Reisenfeld, D.B., Wiens, R.C., Barraclough, B.L., Steinberg, J.T., Neugebauer, M., Raines, J., Zurbuchen, T.H., 2013. Solar wind conditions and composition during the Genesis mission as measured by in situ spacecraft. Space Sci. Rev. 175, 125-164.

Robbins, D.E., Hundhausen, A.J., Bame, S.J., 1970. Helium in solar wind. J. Geophys. Res. 75, 1178-1187.

Schwenn, R., 1983. The "average" solar wind in the inner heliosphere: structures ans slow variations. In: NASA CP 2280 Solar Wind Five, 489-507.

Steinitz, R., Eyni, M., 1980. Global properties of the solar wind. 1. The invariance of the momentum flux density. Astrophys. J. 241, 417-424.

Vermeesch, P., 2018. IsoplotR: a free and open toolbox for geochronology. Geoscience Frontiers 9, 1479-1493.

Vogel, N., Heber, V.S., Baur, H., Burnett, D.S., Wieler, R., 2011a. Argon, krypton, and xenon in the bulk solar wind as collected by the Genesis mission. Geochim. Cosmochim. Acta 75, 3057-3071.

Vogel, N., Baur, H., Burnett, D.S., Maden, C., Wieler, R., 2011b. Argon, krypton, and xenon in three solar wind regimes as collected by Genesis. 42nd Lunar and Planetary Science Conference. Lunar and Planetary Institute, Houston, #1767.

von Steiger, R., Zurbuchen, T.H., McComas, D.J., 2010. Oxygen flux in the solar wind: Ulysses observations. Geophys. Res. Lett. 37, L22101.

Wieler, R., 2002. Noble gases in the solar system. Rev. Mineral. Geochem. 47, 29-70.

Wieler, R., 2016. Do lunar and meteoritic archives record temporal variations in the composition of solar wind noble gases and nitrogen? A reassessment in the light of Genesis data. Chem Erde-Geochem. 76, 463-480.

Wieler, R., Baur, H., 1995. Fractionation of Xe, Kr, and Ar in the solar corpuscular radiation deduced by closed system etching of lunar soils. Astrophys. J. 453, 987-997.

Wieler, R., Kehm, K., Meshik, A.P., Hohenberg, C.M., 1996. Secular changes In the xenon and krypton abundances in the solar wind recorded in single lunar grains. Nature 384, 46-49.

Zahnle, K.J., Gacesa, M., Catling, D.C., 2019. Strange messenger: A new history of hydrogen on Earth, as told by Xenon. Geochim. Cosmochim. Acta 244, 56-85.

Zurbuchen, T.H., Weberg, M., von Steiger, R., Mewaldt, R.A., Lepri, S.T., Antiochos, S.K., 2016. Composition of coronal mass ejections. Astrophysical Journal 826:10.

Figure 1:

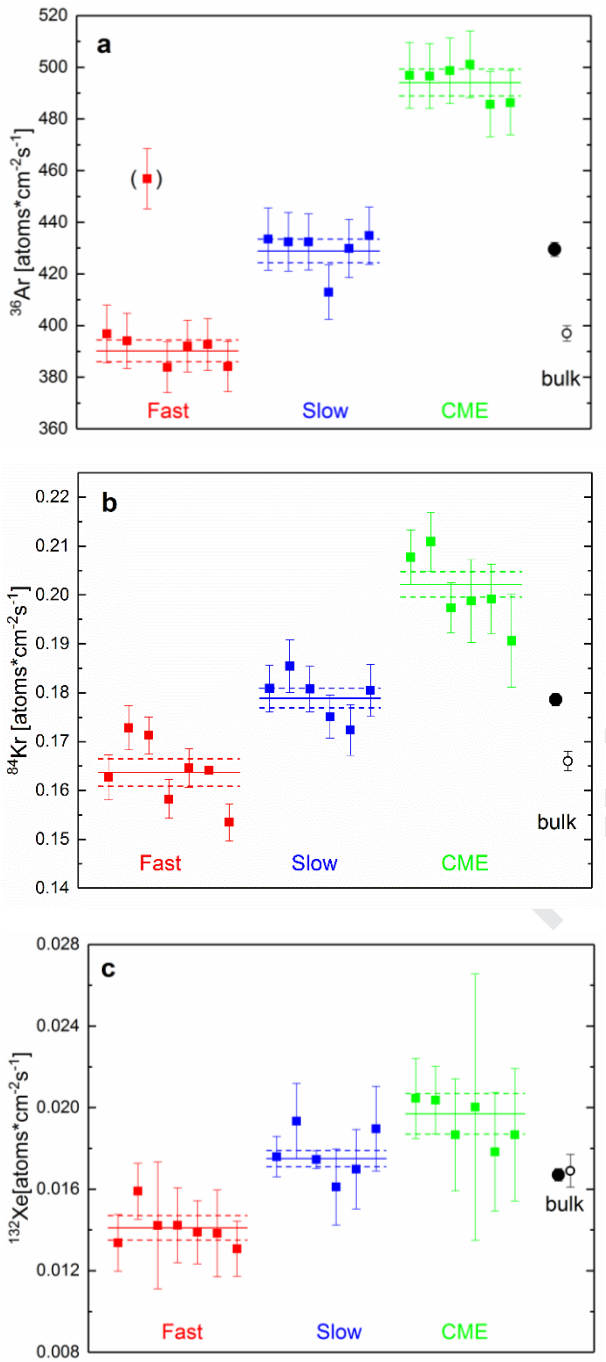

Fig. 1: Fluxes of ^{36}Ar, ^{84}Kr and ^{132}Xe deduced from concentrations in indivdual CZ-Si target samples from the three different solar wind regimes sampled by Genesis (data from Table 1). Weighted averages with one sigma uncertainties given by horizonal solid and dashed bars, respectively (for ^{84}Kr in Fast SW targets, the standard error of the mean based on the data scatter is also shown as dotted lines, see text). Individual analyses also given with one sigma error bars. Fluxes of bulk solar wind calculated from the present regime data given by solid black dots, respective fluxes determined by Vogel et al. (2011a) with bulk SW CZ-Si targets given by open dots with one sigma error bar (cf Table 1).

Figure 2:

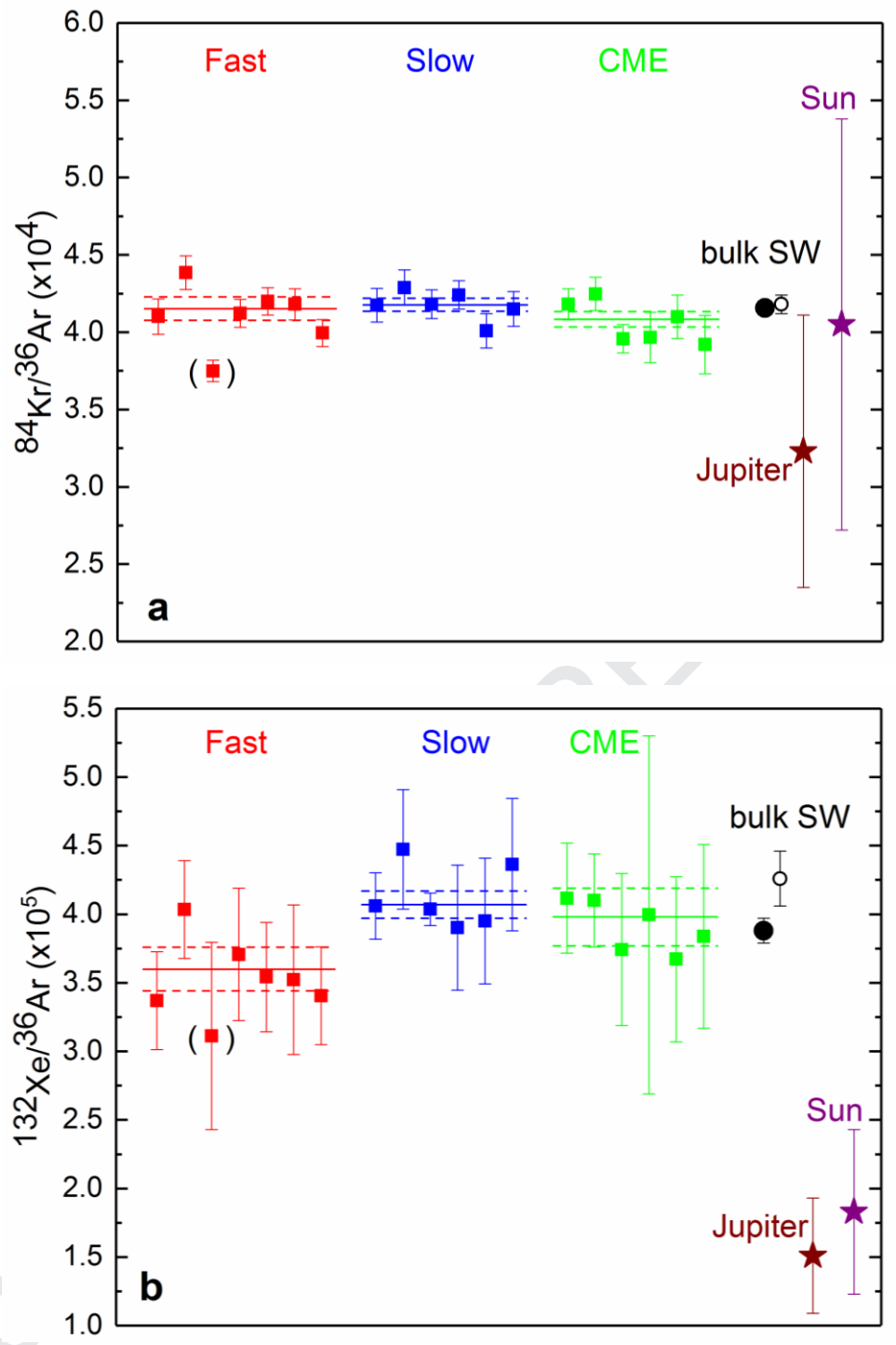

Fig. 2: $^{84}Kr/^{36}Ar$ and $^{132}Xe/^{36}Ar$ element ratios in the three Genesis regimes. Weighted averages with one sigma uncertainties given by horizonal solid and dashed bars, respectively Individual analyses also given with one sigma error bars. Fluxes of bulk solar wind calculated from the present regime data given by solid black dots, respective fluxes determined by Vogel et al. (2011a) with bulk SW CZ-Si targets given by open dots with one sigma error bar (cf Table 1). Values for Sun and Jupiter from Lodders et al. (2009) and Atreya et al. (2003), respectively.

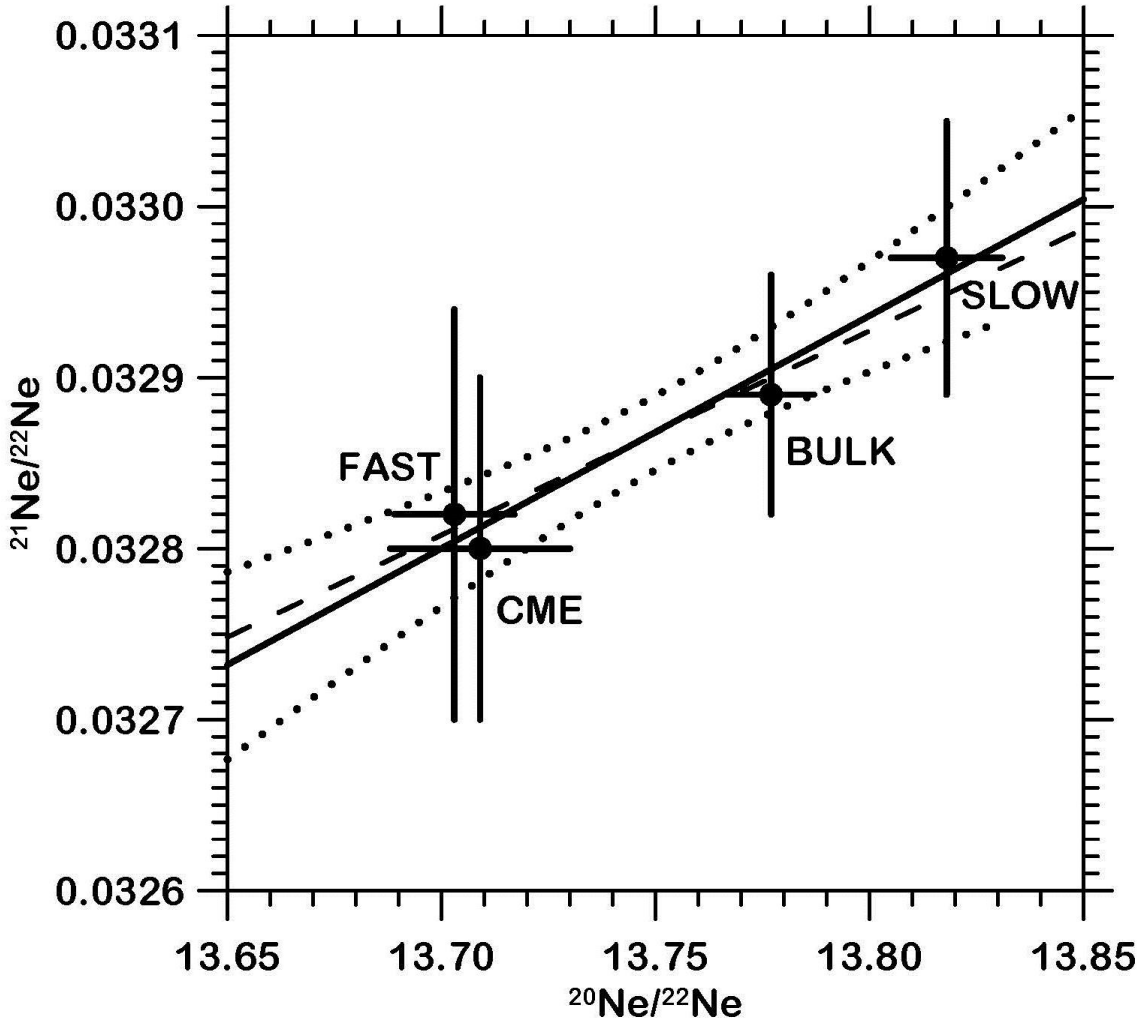

Fig. 3: Average Ne isotopic compositions of bulk solar wind and the three solar wind regimes. Data for bulk solar wind as well as for slow and fast regimes are from Heber et al. (2012), see also Table 3. The straight solid line represents the unweighted fit through all data points, with its 2 σ uncertainty indicated by the dotted lines. The best fit line nearly coincides with the correlation expected for mass-dependent fractionation, shown as dashed line.

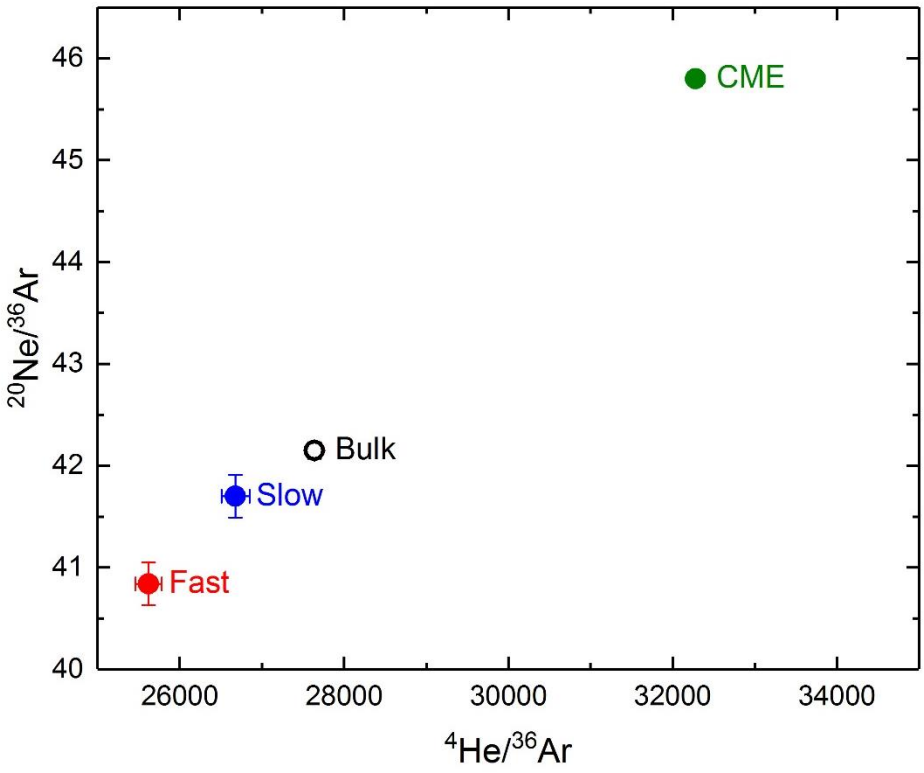

Fig. 4: Average $^{20}Ne/^{36}Ar$ versus $^{4}He/^{36}Ar$ ratios of the DOS targets measured by Heber et al. (2012) sampling the three SW regimes (data from Table 2).

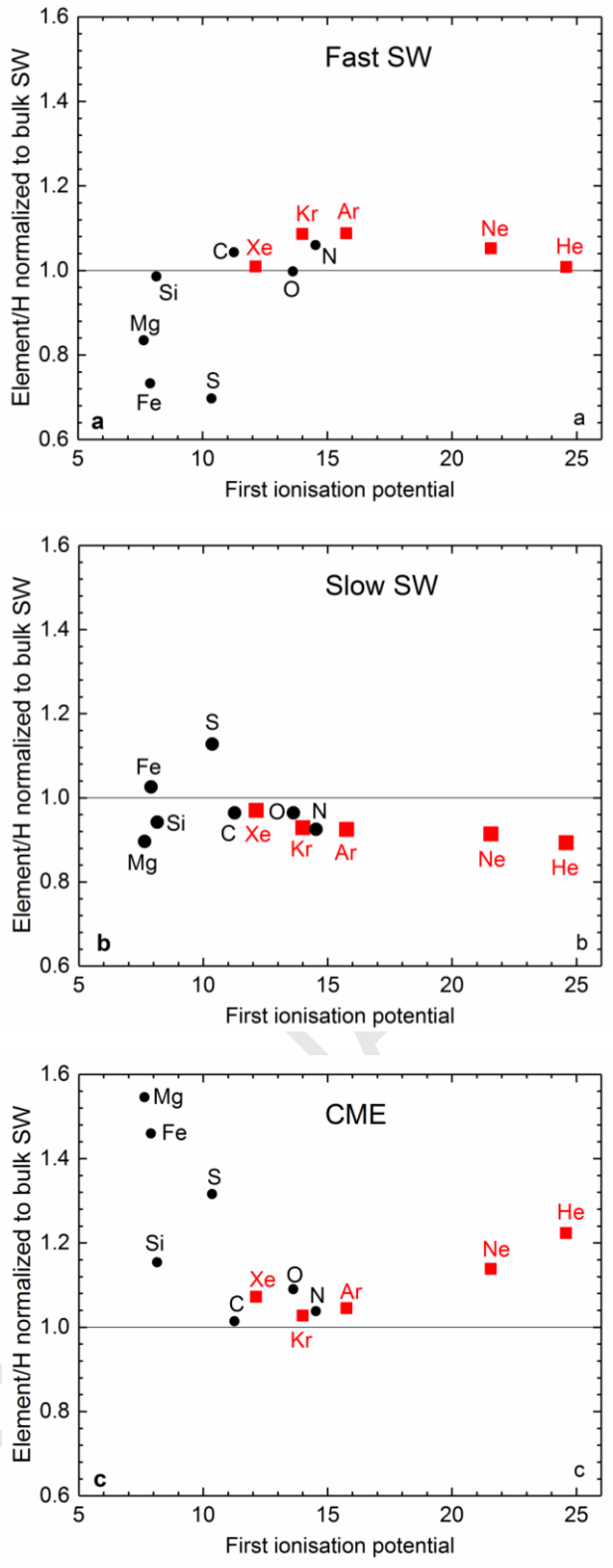

Fig. 5: Relative enrichments or depletions of elements in three SW regimes with respect to hydrogen and normalized to bulk SW values. Black dots represent ACE data from Reisenfeld et al. (2013) for the exposure periods of the respective Genesis regime collectors, red squares noble gas data from this work (Table 4, lower part). Noble gases are connected to the other elements through the He abundances given in this work as well as by Reisenfeld et al. (2013).

Table 1: Ar, Kr & Xe fluxes and elemental ratios (atoms/atom) in Genesis CZ-Si regime targets

Sample Code	area [cm^2]	^{36}Ar	±	^{84}Kr	±	^{132}Xe	±	^{84}Kr/^{36}Ar (x10^4)	± (x10^4)	^{132}Xe/^{36}Ar (x10^5)	± (x10^5)
Fast SW											
60703-H	0.475	396.8	11.1	.1628	.0046	.0134	.0014	4.102	.114	3.37	.36
60799-H	0.253	394.1	10.7	.1728	.0045	.0159	.0014	4.385	.109	4.04	.36
30947-H	0.317	*456.8*	*11.7*	.1713	.0037	.0142	.0031	*3.750*	*.069*	*3.11*	*.68*
60706-H	0.333	383.9	9.8	.1583	.0040	.0142	.0018	4.123	.090	3.71	.48
21010-H	0.310	392.1	10.0	.1646	.0040	.0139	.0015	4.199	.088	3.54	.40
60973-H	0.211	392.7	10.0	.1642	.0044	.0138	.0021	4.180	.101	3.52	.54
60792-H	0.383	384.1	9.7	.1535	.0038	.0131	.0014	3.995	.087	3.40	.36
average Fast		390.2	4.2	.1637	.0028	.0141	.0006	4.152	.039	3.60	.16
MSWD		0.28		2.91		0.43		1.70		0.46	
Slow SW											
50826-L	0.489	433.5	12.1	0.1809	.0048	0.0176	.0010	4.174	.109	4.06	0.24
60662-L	0.329	432.4	11.4	0.1855	.0054	0.0193	.0019	4.289	.115	4.47	0.44
60652-L	0.324	432.4	10.9	0.1808	.0046	0.0175	.0004	4.180	.093	4.04	0.12
60685-L	0.401	412.9	10.6	0.1751	.0044	0.0161	.0019	4.241	.092	3.90	0.46
50901-L	0.313	429.9	11.2	0.1723	.0051	0.0170	.0019	4.009	.110	3.95	0.46
60592-L	0.295	434.8	11.1	0.1805	.0053	0.0190	.0021	4.150	.111	4.36	0.48
average Slow		428.9	4.6	0.1789	.0020	0.0175	.0004	4.177	.042	4.07	.10
MSWD		0.58		0.87		0.45		0.77		0.29	
CME SW											
41001-E	0.527	496.9	12.8	0.2077	.0037	0.0205	.0020	4.181	.101	4.12	.40
60708-E	0.396	496.6	12.5	0.2109	.0043	0.0204	.0017	4.247	.108	4.10	.34
60707-E	0.345	498.7	12.7	0.1974	.0033	0.0187	.0027	3.958	.091	3.74	.55
60389-E	0.344	501.2	13.0	0.1988	.0075	0.0200	.0065	3.966	.163	4.00	1.31
41012-E	0.292	485.7	12.6	0.1991	.0059	0.0178	.0029	4.100	.140	3.67	.60
60782-E	0.366	486.3	12.4	0.1906	.0087	0.0187	.0032	3.920	.189	3.84	.67
average CME		494.1	5.2	0.2022	.0026	0.0197	.0010	4.084	.049	3.98	.21
MSWD		0.27		1.16		0.19		1.30		0.15	
bulk SW, this work[1]		429.5	2.7	0.1786	.0012	0.0167	.0004	4.157	.028	3.88	.09
bulk SW, CZ-Si bulk[2]		397	3	0.166	.002	0.0169	.0008	4.181	.060	4.26	.20
bulk SW, Al target[3]		366	6	0.147	.007	0.0156	.0005	4.005	.20	4.26	.15
solar[4]								4.05	1.33	1.83	.60

All samples are CZ-Si. Extracted areas are given in [cm^2], fluxes of ^{36}Ar, ^{84}Kr & ^{132}Xe in [atoms*cm^{-2}s^{-1}], calculated from measured concentrations and regime exposure durations of 313.01 days (Fast SW), 333.67 days (Slow SW) and 193.25 days (CME SW), respectively (Reisenfeld et al., 2013). Stated uncertainties (for clarity given with the same number of significant digits as the respective values) are 1σ. Weighted averages and Mean Square Weighted Deviations (MSWD) calculated with IsoplotR (Vermeesch 2018), with the ^{36}Ar value of Fast SW target #3 and the corresponding ratios (in italics) rejected as outliers. MSWD values indicate an overdispersion of the ^{84}Kr data for Fast SW, whereas MSWD values of the ^{132}Xe/^{36}Ar ratios indicate an underdispersion in all regimes, i. e. a likely overestimated uncertainty of the average Xe/Ar elemental ratios (see text).

1) bulk SW values as calculated from regime data weighted by respective exposure durations

2) bulk SW values measured with Genesis Bulk-SW CZ-Si targets (Vogel et al., 2011a), uncertainties of standard gases not included here.

3) bulk SW values measured with Genesis Bulk SW Al targets (Meshik et al., 2014; see also Meshik et al., 2009)

4) solar values from Lodders et al. (2009).

.

.

Table 2: He, Ne, & Ar fluxes and elemental ratios in Genesis DOS regime targets

	^{4}He ($x10^{7}$)	± ($x10^{7}$)	^{20}Ne ($x10^{4}$)	± ($x10^{4}$)	^{36}Ar	±	^{4}He/^{36}Ar	±	^{20}Ne/^{36}Ar	±
average Bulk SW[1]	1.125	.003	1.716	.007	407	2	27640	80	42.15	.08
average Fast SW	0.960	.002	1.529	.007	375	4	25610	310	40.78	.50
average Slow SW	1.093	.004	1.708	.009	410	2	26680	90	41.67	.11
CME SW										
60374-1 E	1.513	.001	2.150	.010	469	2	32340	120	45.95	.27
60374-2 E	1.522	.001	2.162	.009	469	2	32540	130	46.22	.26
60374-3 E	1.514	.001	2.145	.008	472	2	32100	110	45.47	.23
average CME	1.516	.005	2.152	.009	470	3	32330	220	45.88	.38
bulk SW calc.[2]	1.141	.002	1.743	.005	411	2	27580	140	42.31	.24
solar[3]							26610	7000	39.0	14

All samples are DOS (CME target: NASA Code 60374). Experimental procedures and further details are given in Heber et al. (2012); data from mass spectrometer "Albatros" reported here. Heber et al. (2012) also give the full data for Fast and Slow SW regimes and Bulk SW targets. Fluxes are given in [atoms*cm^{-2}s^{-1}]. Stated uncertainties represent standard deviations of individual analyses.
1) average bulk SW measured with Genesis bulk targets (Heber et al. 2009, 2012)
2) average Bulk SW calculated with regime data given here
3) solar values from Lodders et al. (2009)

Table 3: He, Ne, & Ar isotopic ratios in three Genesis CME and other regime targets

	^{3}He/^{4}He ($x10^{-4}$)	± ($x10^{-4}$)	^{20}Ne/^{22}Ne	±	^{21}Ne/^{22}Ne	±	^{36}Ar/^{38}Ar	±
CME targets (this work)								
60374-1 E	4.665	.008	13.70	.03	.0331	.0002	5.459	.016
60374-2 E	4.624	.012	13.73	.02	.0329	.0003	5.475	.010
60374-3 E	4.657	.012	13.72	.02	.0325	.0003	5.460	.007
CME average	4.649	.021	13.71	.02	.0328	.0001	5.465	.009
Bulk[1]	4.645	.008	13.777	.010	.03289	.00007	5.470	.003
Slow[1]	4.768	.009	13.818	.013	.03297	.00008	5.479	.003
Fast[1]	4.478	.011	13.703	.014	.03282	.00012	5.451	.004

All analyses made on the same DOS CME targets listed in Table 2. Stated uncertainties of the DOSdata represent 1σ errors of individual analyses. The lines "average (δ)" represent deviations in ‰ of the average isotopic ratios relative to the average bulk SW values given by Heber et al. (2012), with stated uncertainties representing standard errors of the mean values.
1: Average isotopic ratios of Bulk, Slow and Fast SW targets from Heber et al. (2012).

Table 4: Relative proton and noble gas fluxes in different SW regimes

	H	^{4}He	±	^{20}Ne	±	^{36}Ar[1]	±	^{36}Ar[2]	±	^{84}Kr	±	^{132}Xe	±
bulk SW	1	1		1		1		1		1		1	
Fast SW	0.847	0.841	.004	0.878	.006	0.912	.011	0.905	.009	0.920	.008	.845	.041
Slow SW	1.133	0.958	.004	0.980	.006	0.998	.007	1.004	.009	0.998	.009	1.048	.035
CME	1.001	1.328	.005	1.234	.008	1.142	.009	1.147	.011	1.132	.013	1.180	.066

noble gas to proton flux ratio in SW regimes normalized to ratio in bulk SW

	^{4}He	^{20}Ne	^{36}Ar	^{84}Kr	^{132}Xe
Bulk SW	1	1	1	1	1
Fast SW	1.008	1.052	1.088	1.086	1.01
Slow SW	0.893	0.914	0.925	0.929	0.97
CME	1.223	1.138	1.045	1.027	1.07

All noble gas fluxes in the upper part of the table normalized to bulk SW values (Tables 1 & 2), with the weighted regime target fluxes taken as Bulk SW values. Relative hydrogen fluxes are from the Genesis Ion Monitor (Reisenfeld et al., 2013); the absolute flux for bulk SW is $2.80*10^{8}$ H*cm^{-2}s^{-1}.

1) Ar fluxes from DOS targets (Table 2)

2) Ar fluxes from Si targets (Table 1)

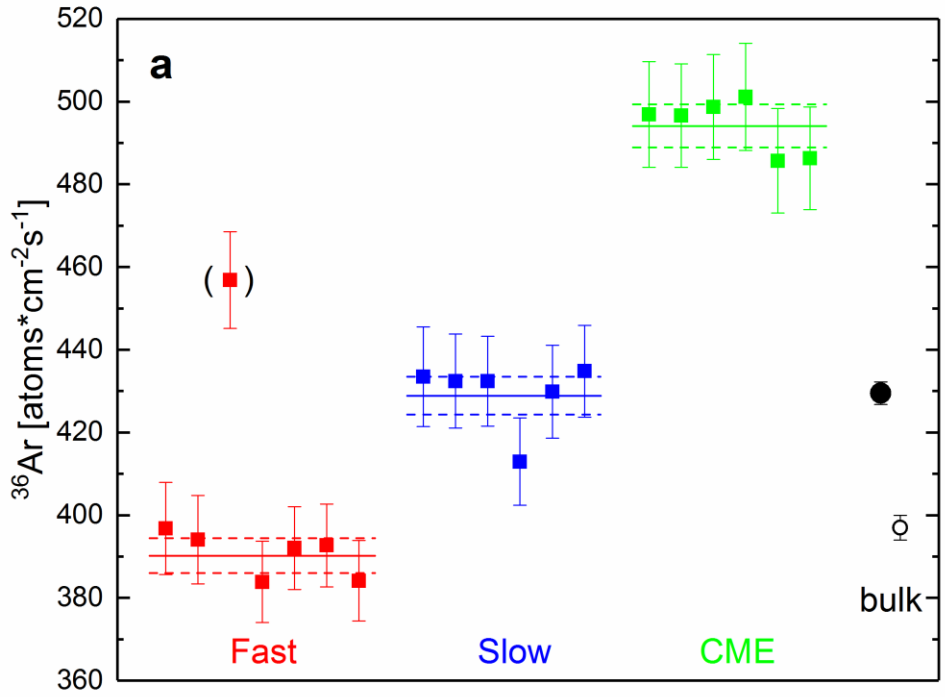
a
520
500
480
460
440
420
400
380
360
^{36}Ar [atoms*cm^{-2}s^{-1}]
( )
bulk
Fast
Slow
CME

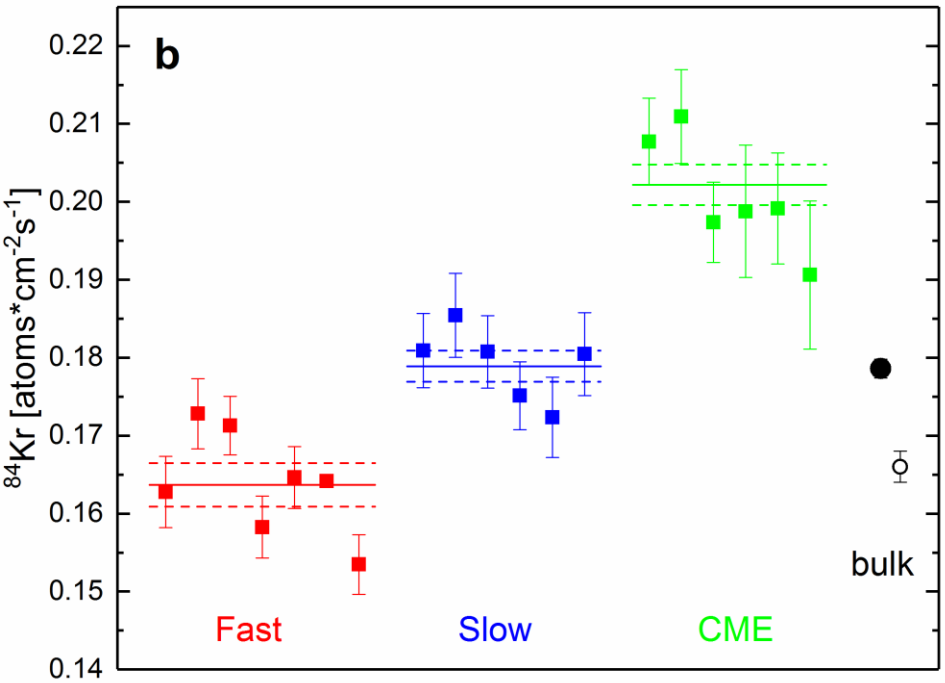
b
0.22
0.21
0.20
0.19
0.18
0.17
0.16
0.15
0.14
^{84}Kr [atoms*cm^{-2}s^{-1}]
bulk
Fast
Slow
CME

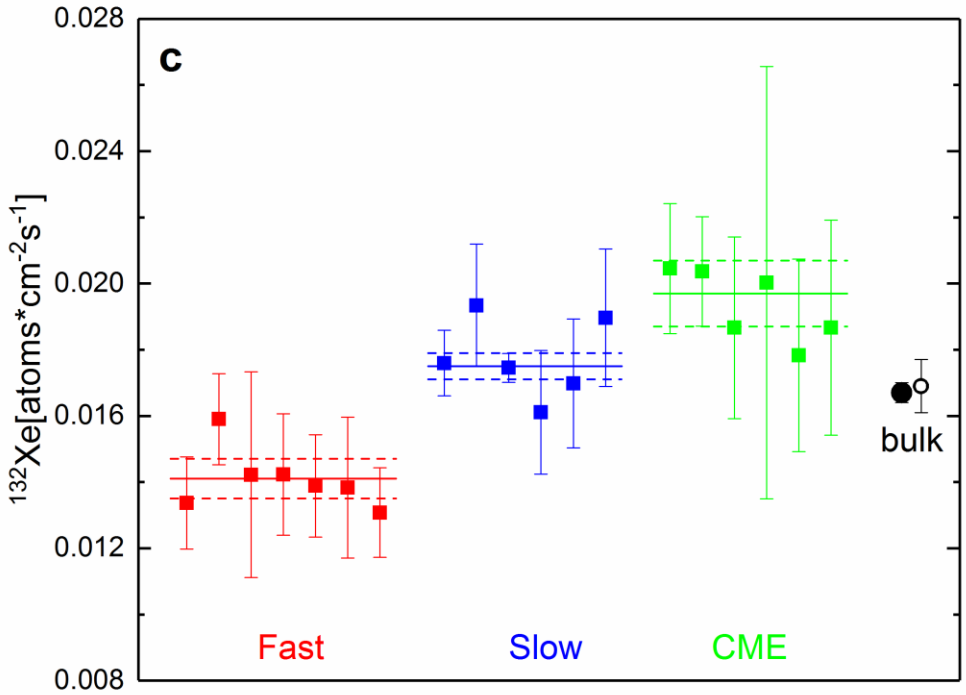
c
0.028
0.024
0.020
0.016
0.012
0.008
^{132}Xe[atoms*cm^{-2}s^{-1}]
Fast
Slow
CME
bulk

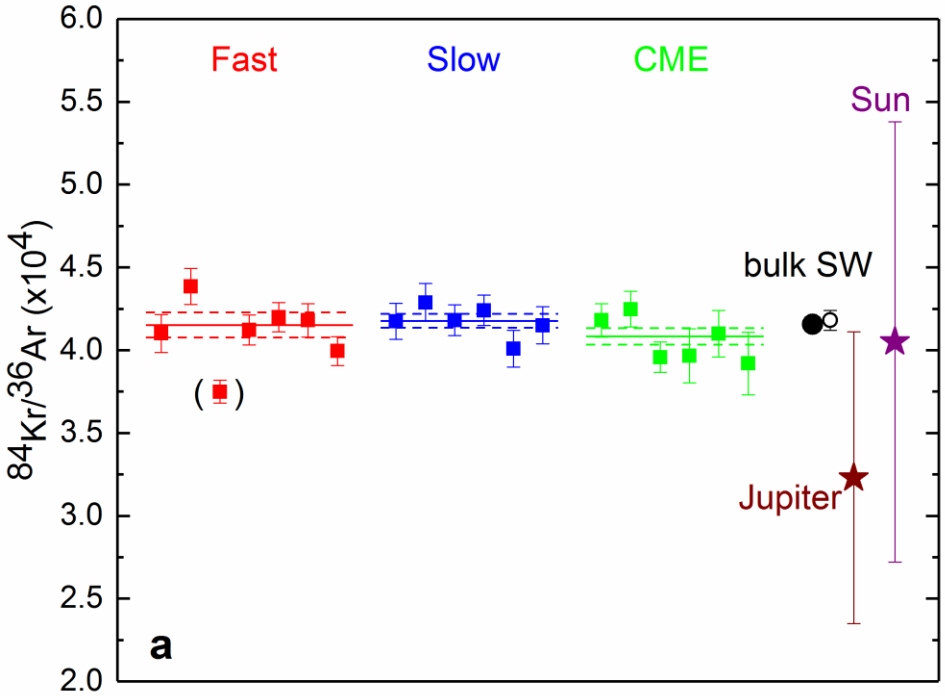
a
6.0
5.5
5.0
4.5
4.0
3.5
3.0
2.5
2.0
^{84}Kr/^{36}Ar (x10^4)
Fast
Slow
CME
Sun
bulk SW
Jupiter

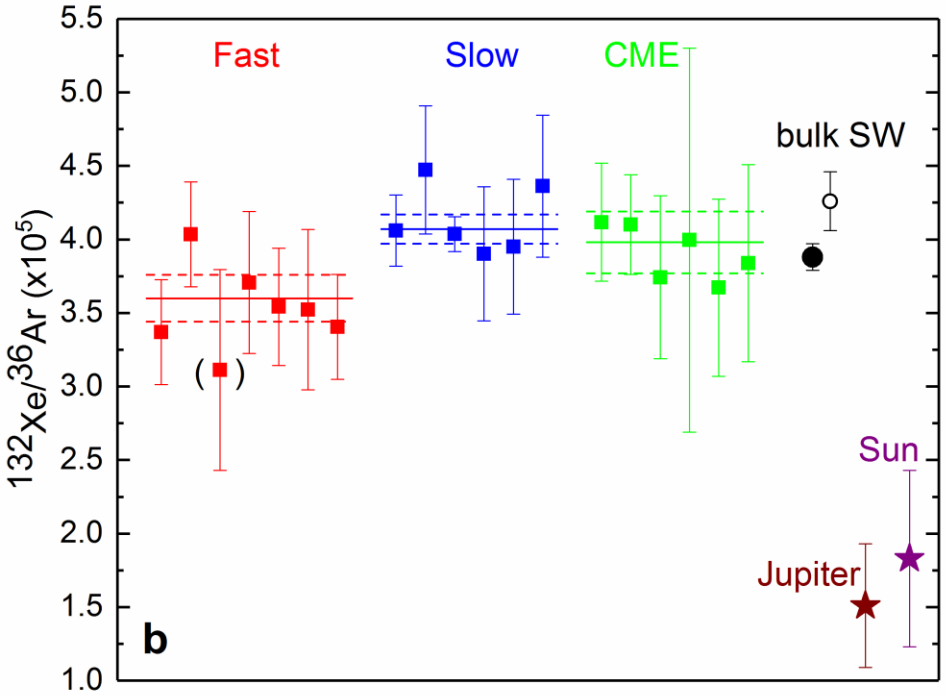

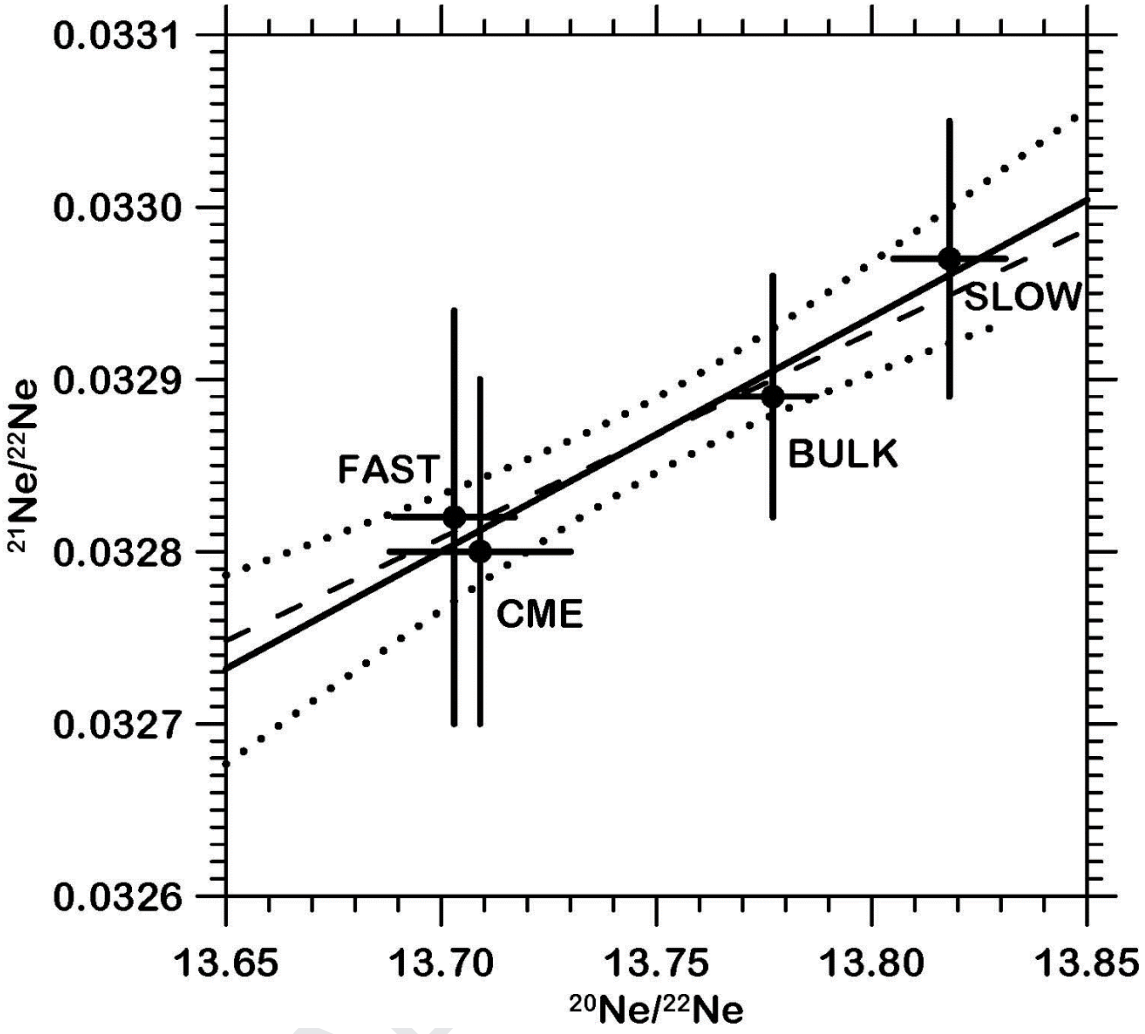
0.0331
0.0330
0.0329
0.0328
0.0327
0.0326
$^{21}Ne/^{22}Ne$
13.65
13.70
13.75
13.80
13.85
$^{20}Ne/^{22}Ne$
FAST
CME
BULK
SLOW

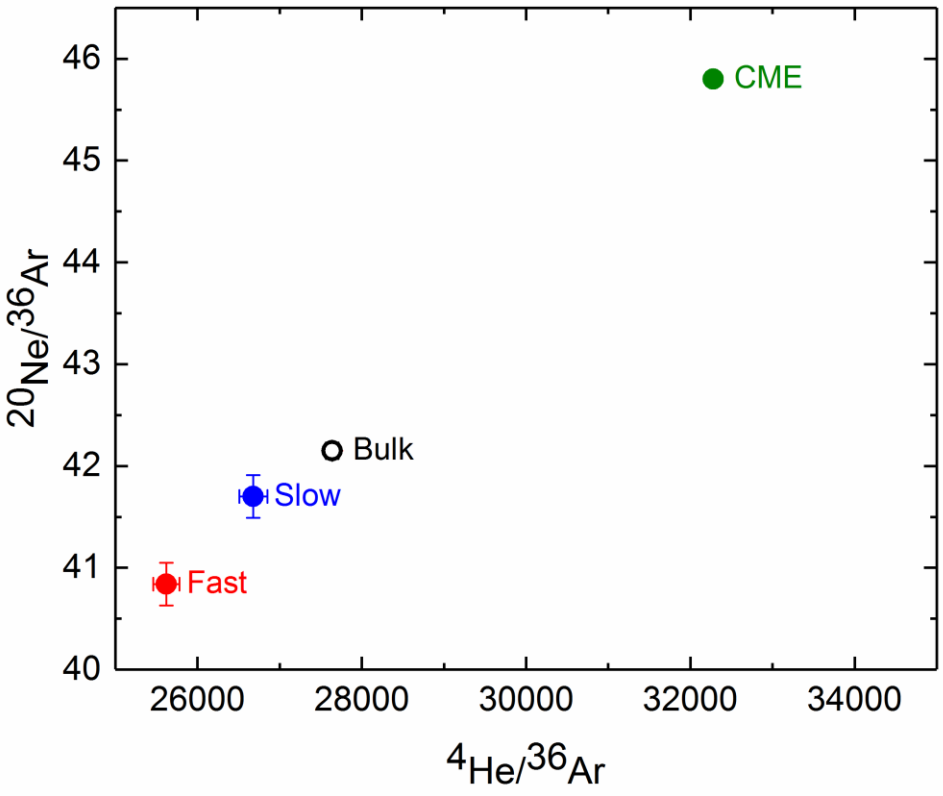
CME
Bulk
Slow
Fast
$^{20}Ne/^{36}Ar$
$^{4}He/^{36}Ar$
46
45
44
43
42
41
40
26000
28000
30000
32000
34000

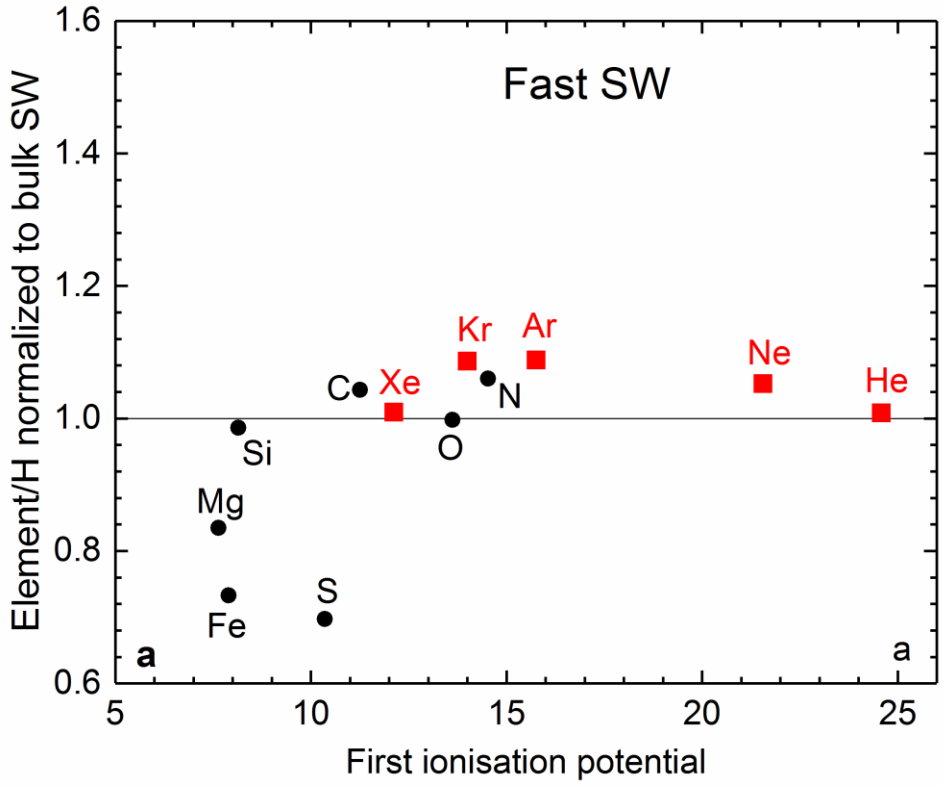
Fast SW
Element/H normalized to bulk SW
First ionisation potential
Kr
Ar
Ne
He
Xe
C
N
O
Si
Mg
S
Fe
a
a
1.6
1.4
1.2
1.0
0.8
0.6
5
10
15
20
25

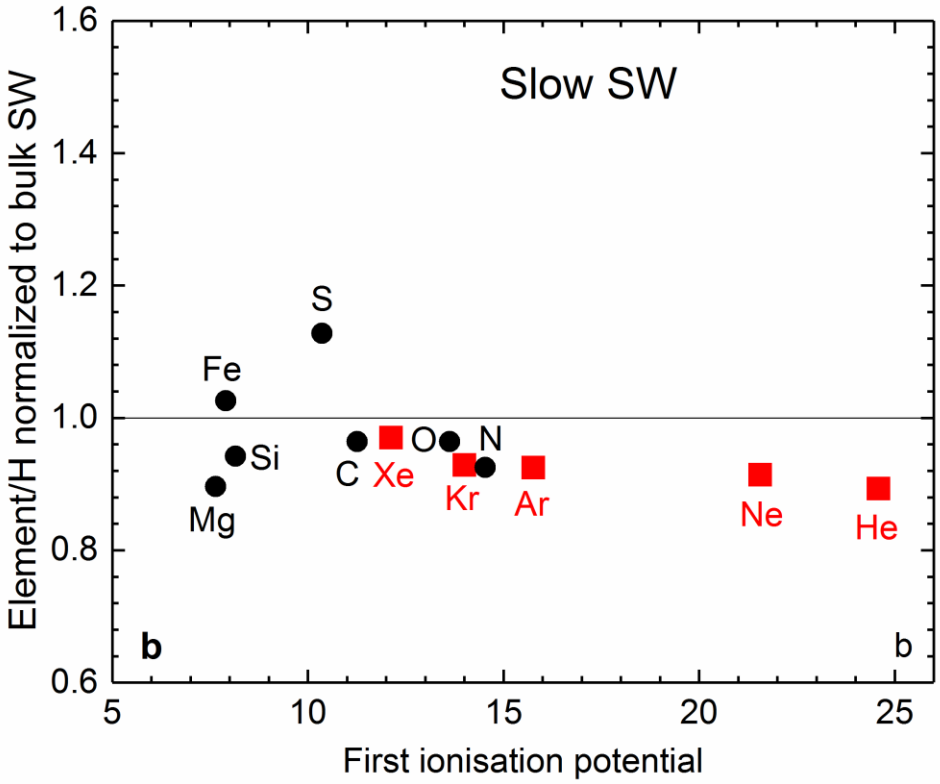
Slow SW
Element/H normalized to bulk SW
First ionisation potential
1.6
1.4
1.2
1.0
0.8
0.6
5
10
15
20
25
S
Fe
Si
Mg
C
O
N
Xe
Kr
Ar
Ne
He
b
b

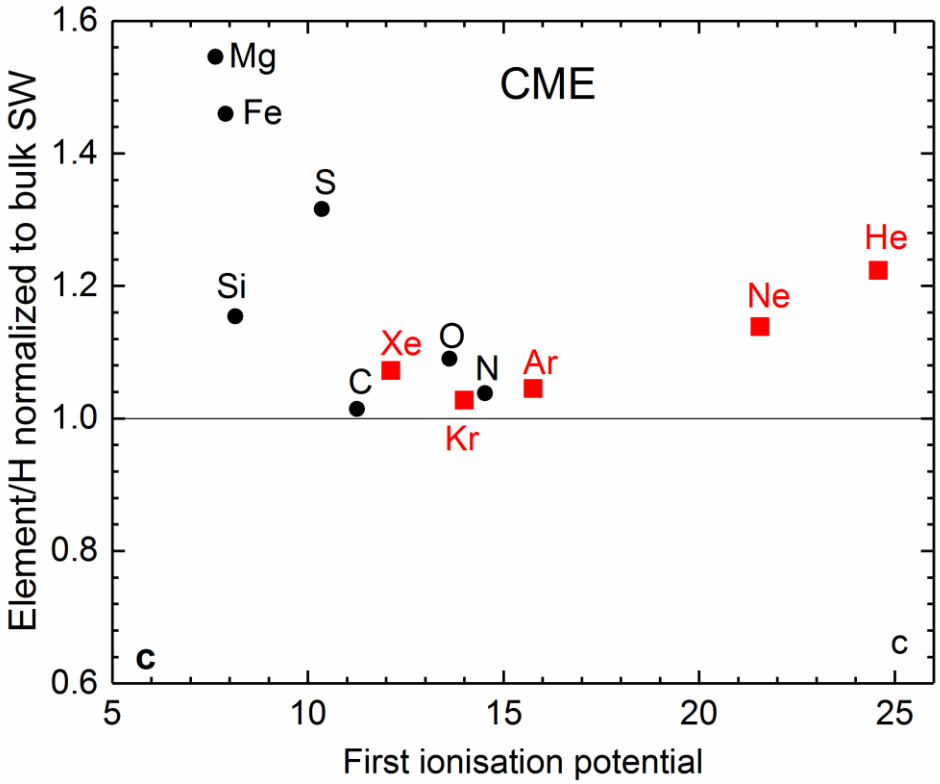
CME
Element/H normalized to bulk SW
First ionisation potential
1.6
1.4
1.2
1.0
0.8
0.6
5
10
15
20
25
Mg
Fe
S
Si
C
Xe
O
N
Kr
Ar
Ne
He
c
c